Journal of Quantitative Spectroscopy & Radiative Transfer 114 (2013) 29–41

Contents lists available at SciVerse ScienceDirect

Journal of Quantitative Spectroscopy & Radiative Transfer

journal homepage: www.elsevier.com/locate/jqsrt

Assignment and rotational analysis of new absorption bands of carbon dioxide isotopologues in Venus spectra

S. Robert [a,*], Yu.G. Borkov [b], J. Vander Auwera [c,1], R. Drummond [a], A. Mahieux [a], V. Wilquet [a], A.C. Vandaele [a], V.I. Perevalov [b], S.A. Tashkun [b], J.L. Bertaux [d,e]

[a] Belgian Institute for Space Aeronomy, 3 Ave Circulaire, B-1180 Brussels, Belgium
[b] Laboratory of Theoretical Spectroscopy, V. E. Zuev Institute of Atmospheric Optics of Siberian Branch of the Russian Academy of Sciences, 1, Akademician Zuev sq., 634021 Tomsk, Russia
[c] Service de Chimie Quantique et Photophysique CP160/09, Université Libre de Bruxelles, 50 Av. F.D. Roosevelt, B-1050 Bruxelles, Belgium
[d] LATMOS, 11 Bd d'Alembert, 78280 Guyancourt, France
[e] IPSL, Université UVSQ, Guyancourt, France

ARTICLE INFO

Article history:
Received 5 April 2012
Received in revised form
22 August 2012
Accepted 23 August 2012
Available online 31 August 2012

Keywords:
Carbon dioxide
Isotopologues
Infrared
Line positions
Spectroscopic constants
Venus atmosphere

ABSTRACT

We present absorption bands of carbon dioxide isotopologues, detected by the Solar Occultation for the Infrared Range (SOIR) instrument on board the Venus Express Satellite. The SOIR instrument combines an echelle spectrometer and an Acousto-Optical Tunable Filter (AOTF) for order selection. It performs solar occultation measurements in the Venus atmosphere in the IR region (2.2–4.3 μm), at a resolution of 0.12–0.18 cm^{-1}. The wavelength range probed by SOIR allows a detailed chemical inventory of the Venus atmosphere above the cloud layer (65–150 km) to be made with emphasis on the vertical distributions of gases. Thanks to the SOIR spectral resolution, a new CO_2 absorption band was identified: the 21101–01101 band of $^{16}O^{12}C^{18}O$ with R branch up to $J=31$. Two other previously reported bands were observed dispelling any doubts about their identifications: the 20001–00001 band of $^{16}O^{13}C^{18}O$ [Villanueva G, et al. J Quant Spectrosc Radiat Transfer 2008;109:883–894] and the 01111–00001 band of $^{16}O^{12}C^{18}O$ [Villanueva G, et al. J Quant Spectrosc Radiat Transfer 2008;109:883–894 and Wilquet V, et al. J Quant Spectrosc Radiat Transfer 2008;109:895–905]. These bands were analyzed, and spectroscopic constants characterizing them were obtained. The rotational assignment of the 20001–00001 band was corrected. The present measurements are compared with data available in the HITRAN database.

1. Introduction

Interest in the composition of the Venus atmosphere began as early as Lomonosov's report [1], from the observations of the 1671 transit, that Venus had an atmosphere and the later discovery by Adams and Dunham [2] that its main constituent was carbon dioxide (CO_2). Venus has an atmosphere very different from that of the Earth: it is much denser, heavier, and extends to a much higher altitude. Despite the harsh conditions on Venus' surface, the atmospheric pressures and temperatures at ~50–65 km levels in Earth and Venus are comparable. Measurements of the chemical and isotopic composition of the Venus atmosphere provide essential boundary conditions for theories and models describing the formation of the planet Venus and the origin and evolution of its atmosphere.

The SOIR (Solar Occultation in the IR) spectrometer is an extension mounted on top of the SPICAV instrument [3], one of the seven instruments on board Venus Express,

* Corresponding author.
E-mail address: severine.robert@aeronomie.be (S. Robert).
[1] Senior Research Associate with the Fonds de la Recherche Scientifique (F.R.S.-FNRS, Belgium).

0022-4073/$ - see front matter © 2012 Elsevier Ltd. All rights reserved.
http://dx.doi.org/10.1016/j.jqsrt.2012.08.023

a planetary mission of the European Space Agency (ESA) launched in November 2005 and inserted into orbit around Venus in April 2006 [4]. SOIR [5] was developed at IASB/BIRA, which is also responsible for planning its operations and for the scientific interpretation of its observations. It is designed to measure the atmospheric transmission in the IR (2.2–4.3 μm) at high resolution (around 0.15 cm^{-1}) using the solar occultation technique. This technique [6] allows the derivation of unique information about the vertical structure and composition of the Venus mesosphere to be made. SOIR is the first high-resolution mid-IR spectrometer onboard a spacecraft investigating the Venus atmosphere. The wavelength range probed by SOIR enables a sensitive search for any minor molecular species from the top of the clouds up to an altitude of about 175 km to be carried out, and leads to detailed information on the vertical composition and structure of the Venus atmosphere above the clouds.

As, for example, shown by the work of Mandin [7], special emphasis can be placed on the detection of new bands of CO_2 and its isotopologues which cannot be observed on Earth or in the laboratory because of their weak intensity, but are seen in Venus spectra because CO_2 is present in large quantities and because of the optical path length. Recently, a new band of isotopic CO_2 near 3.3 μm was identified from SOIR measurements of the Venus atmosphere [8] and Earth based measurements of Mars [9]. This raised the possibility to observe other new isotopic CO_2 bands in the wavelength range of the SOIR instrument and a systematic search for such bands was therefore initiated.

In this work (TW) we report the observation of a new band centered at 2791.53 cm^{-1}, assigned as the 21101–01101 band of $^{16}O^{12}C^{18}O$. Two other bands, namely, the 20001–00001 band of $^{16}O^{13}C^{18}O$ centered at 2701.95 cm^{-1} and the 01111 − 00001 band of $^{16}O^{12}C^{18}O$ centered at 2982.12 cm^{-1}, were already reported in [8] and [9], respectively. The rotational structure of the 20001–00001 band was observed by Villanueva et al. [10], who assigned the observed lines as P23–P3. In the CDSD-296 databank [11], these lines are assigned as R4–R24: this latter assignment is used in the present work. For the 01111–00001 band, we analyzed an extended set of observed line positions.

Note that the usual vibrational notation for carbon dioxide is used throughout the paper, namely v_1, v_2, l_2, v_3, r. v_1, v_2, v_3 are the quantum numbers associated with the three modes of vibration (v_1 is the symmetric stretch, v_2 is the bending mode and v_3 is the antisymmetric stretch mode), l_2 is the quantum number associated with the angular momentum induced by the doubly degenerate bending mode v_2, and can take the value v_2, v_2–2, v_2–4,… The last label, r, is a ranking index, which numbers the different states of a Fermi polyad $2v_1+v_2=const$ in descending energy order. The index r runs from 1 to v_1+1 [12].

2. Measurements

The instrument [3,5] and its in-flight performance [13], including data handling, onboard background subtraction, calibrations of the AOTF and the echelle spectrometer, have already been extensively described, whereas the retrieval technique and some results are discussed in the papers by Vandaele et al. [6] and Mahieux et al. [14,15]. SOIR is an echelle grating spectrometer operating in the IR, combined with an AOTF for the selection of the diffraction grating orders. The SOIR detector has 320 columns of pixels along the wavenumber axis and 256 rows along the spatial axis. To avoid saturation, short integration times are used (20–30 ms), depending on the wavelength at which the measurement is taken. The background signal is measured and subtracted onboard. In order to improve the signal-to-noise ratio (SNR), a number of measurements can be accumulated as long as the total measuring time remains below 250 ms. Due to telemetry limitations, only 8 spectra, each 320 pixels long, can be downloaded per second. During the observation periods (i.e. per orbit), these 8 spectra are taken in four different diffraction orders (4 different radio-frequencies applied to the AOTF), each corresponding to two large bins of 16 or 12 rows on the detector.

The instrument features lead to a division of the investigated spectral range (2256–4369 cm^{-1}) into 94 small wavenumber domains, called diffraction orders. The computed wavenumber interval (cm^{-1}) associated with the detector pixels 0 and 319 for echelle orders 101 to 194 can be found in the literature [5].

In solar occultation mode as performed by SOIR, transmittance spectra are obtained by division of all the spectra recorded during an occultation with a reference spectrum obtained when the light path does not intercept the atmosphere (beginning of sunset or end of sunrise observations). As the light beam probes deeper layers in the atmosphere, two processes reducing the transmittance take place: extinction by aerosols and absorption by trace gases. In general, spectra containing useful information on the Venus atmosphere correspond to tangent heights between 65 km (slightly above the top of the cloud layer) and 175 km.

The three bands analyzed in this paper are observed in the grating diffraction orders 120–121, 124–125 and 131–134. These grating orders correspond to the spectral ranges 2680–2725 cm^{-1}, 2770–2815 cm^{-1} and 2930–3015 cm^{-1}, respectively.

3. Spectral analysis

As the three regions of interest have been recorded many times since the instrument began operations around Venus, we selected a number of spectra for each order to determine the line positions. We chose spectra with good SNR, not affected by saturation and for which the calibration procedure was successful. The SNR has been calculated for all recorded spectra during in-flight calibrations, using the "full Sun spectra" [13].

Considering that the SOIR instrument scans the Venus atmosphere from its top to the top of the Venusian clouds, a selection has to be made in terms of altitudes as well. Specifically, the lower boundary of the considered altitude range was taken to be the altitude at which the atmospheric absorption lines had transmittances reaching zero at their center, before convolution with the instrument resolution function (saturation criterion [14]).

As one vibrational band is too broad to fit in one diffraction order (the free spectral range is around 22 cm^{-1} [5]), we treated each orbit separately, one orbit corresponding to four diffraction orders recorded at various altitudes in the Venus atmosphere. The wavenumber ranges of interest were calibrated semi-automatically using a code called ASIMAT (see Section 3.1), and well-known HCl or HDO lines taken from HITRAN 2008 [16] as reference positions. Each diffraction order of interest was calibrated separately for each orbit during which it was recorded and for each bin (the detector is divided in two bins, as explained in Section 2). Among all the spectra recorded at various altitudes in one diffraction order, only one was chosen to determine the calibration. The calibration function thus determined was then used for all altitudes.

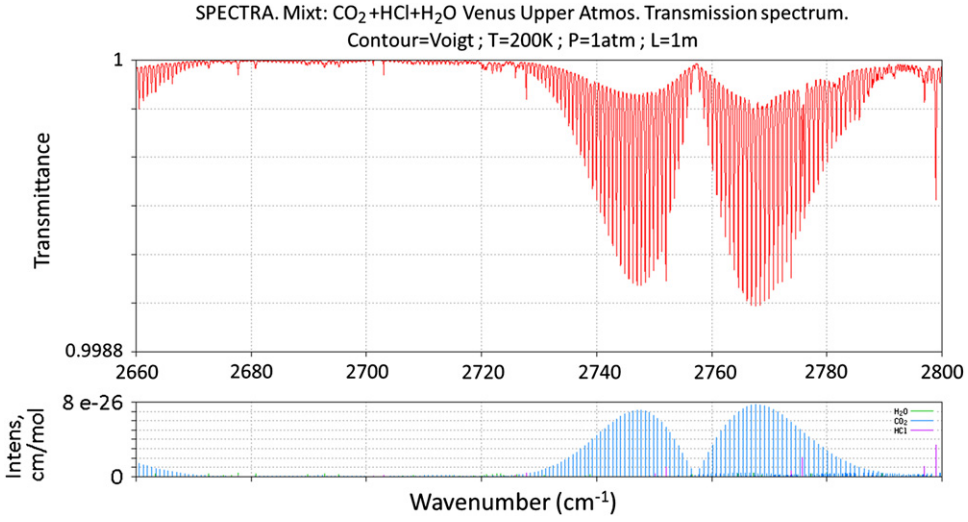

Fig. 1. Synthetic transmittance spectrum for a chosen gas mixture made of 96.5% of CO_2, 2 ppm of H_2O and 100 ppb of HCl with deuterium enriched water [19] and standard isotopic abundances for CO_2 and HCl. The upper panel represents the transmittance under the chosen experimental conditions. The lower panel shows the intensity (integrated absorption cross section at 296 K) of the lines of CO_2 (blue), H_2O (green) and HCl (magenta) included in the calculation. No distinction is made between different isotopologues.

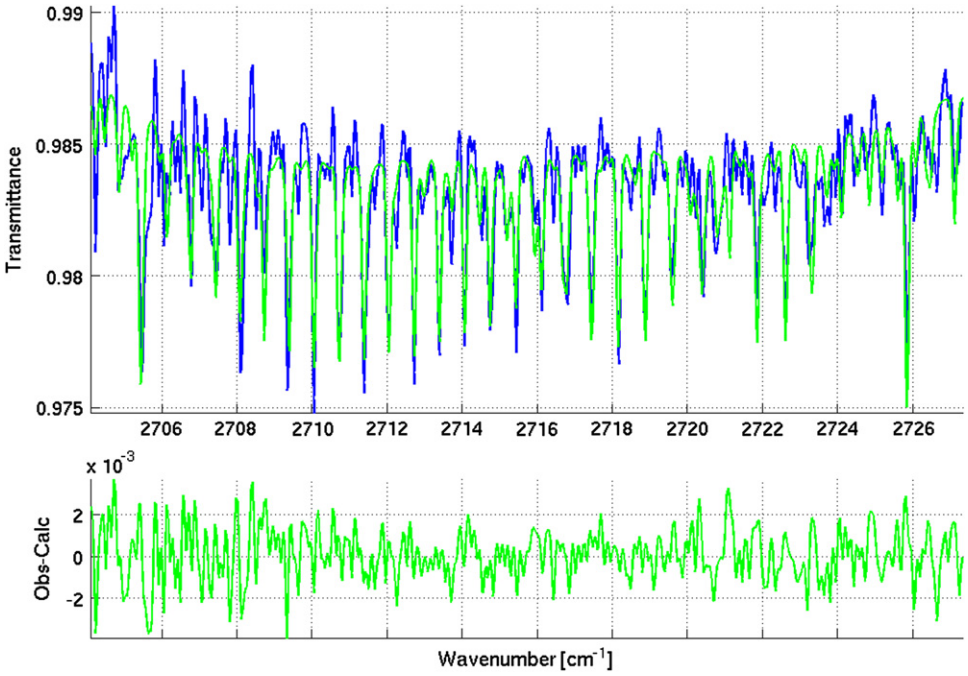

Fig. 2. Spectrum of the R-branch of the 20001–00001 of CO_2 (638) fitted with ASIMAT. In the upper panel, the SOIR spectrum from orbit 244, bin 1 at tangent altitude of 88.4 km and the synthetic spectrum are presented in blue and green respectively. The SNR value of this spectrum is 1606.1. The corresponding residuals are displayed in the lower panel.

3.1. Analysis of the SOIR spectra

As a first step in the systematic search for new vibrational bands, we used the Internet accessible information system SPECTRA [17]. To generate spectra, SPECTRA relies on several databases, such as HITRAN [16] and GEISA [18]. Note that the line positions and line intensities available in HITRAN and GEISA for the three CO_2 bands studied in this work are calculated values from the CDSD-296 databank [11]. We defined a gas mixture similar to that of the upper Venus atmosphere (standard Venusian isotopic abundances of 96.5% for CO_2, 2 ppm for H_2O, deuterium enriched [19], and 100 ppb for HCl) and made simulations in the spectral regions of the SOIR instrument. An example of the spectra thus generated is shown in Fig. 1.

While the search for and assignment of the bands were done using SPECTRA, the line positions were measured with a code called ASIMAT. ASIMAT has been developed by the IASB group [14,15]. Its primary purpose is the retrieval of Venus atmospheric densities and temperature profiles from SOIR spectra, assuming Voigt line profiles calculated using HITRAN 2008 parameters [16] and attempting to take into account all features proper to the SOIR instrument. In the present work, we measured line positions from SOIR spectra using the least squares fitting procedure and modeling of ASIMAT, fixing the pressures and temperatures to the values obtained from the retrieval procedure. Fig. 2 shows an example of such a fit.

The line positions were measured in every non-saturated spectrum. A criterion was defined to select lines above a certain threshold, taking into account the SNR of the concerned orbit. The SNR is automatically calculated for each orbit, each order and each bin by ASIMAT [13]. For each spectrum, we deduced the baseline and the noise strictly speaking, as being the ratio between the observed signal and the SNR of the orbit. Absorption lines were taken into account if the difference between the baseline and their transmittance was greater than twice the value of the noise. The reported line positions are the weighted average of these measurements. The weight associated to each line position is the width of the pixel on which the center of the line was recorded. The associated observational error provided in Tables 1–3 is the average of the widths of the pixel on which the line was recorded.

3.2. Assignments

Comparison of simulated and SOIR spectra in regions of low transmittance revealed three bands of isotopic CO_2, namely the 20001–00001 band of $^{16}O^{13}C^{18}O$, and the 21101–01101 and 01111–00001 bands of $^{16}O^{12}C^{18}O$. Their analysis is described here after.

a) *The 20001–00001 band of $^{16}O^{13}C^{18}O$*
Transitions in this cold band have been observed up to $J=26$ and 31 in the P- and R-branches, respectively (J is the quantum number associated with the total angular momentum of the molecule). As the center of this $\Sigma^+-\Sigma^+$ band is predicted as well as located around 2702 cm^{-1} this band spreads over orders 120 and 121 of the SOIR instrument, as can be seen in Fig. 3.
These two orders have been recorded in several orbits. We used 20 orbits out of 34 for order 120 and 57 orbits

Table 1
Measured and calculated line positions for the 20001–00001 band of CO_2 (638) obtained from SOIR spectra, and comparison with predictions available in HITRAN 2008 [16], which originate from [11].

Line	Calc.[a] (cm^{-1})	Obs. (cm^{-1})	Obs − Calc. (cm^{-1})	Obs. error (cm^{-1})	HITRAN − Calc. (cm^{-1})
P(26)	2682.916	2682.924	0.008	0.070	−0.010
P(25)	2683.644	2683.658	0.014	0.070	−0.012
P(24)	2684.372	2684.367	−0.005	0.070	−0.014
P(23)	2685.101	2685.101	0.000	0.071	−0.015
P(22)	2685.830	2685.841	0.011	0.071	−0.016
P(21)	2686.559	2686.570	0.011	0.071	−0.017
P(20)	2687.288	2687.290	0.002	0.071	−0.018
P(19)	2688.018	2688.027	0.009	0.071	−0.019
P(18)	2688.748	2688.794	0.046	0.071	−0.019
P(17)	2689.479	2689.503	0.024	0.072	−0.019
P(16)	2690.209	2690.233	0.024	0.072	−0.019
P(15)	2690.940	2690.964	0.024	0.072	−0.019
P(14)	2691.672	2691.703	0.031	0.072	−0.019
P(13)	2692.403	2692.401	−0.002	0.072	−0.019
P(12)	2693.136	2693.164	0.028	0.072	−0.018
P(11)	2693.868	2693.899	0.031	0.072	−0.018
P(10)	2694.601	2694.603	0.002	0.073	−0.018
P(9)	2695.334	2695.314	−0.020	0.073	−0.017
P(8)	2696.067	2696.066	−0.001	0.073	−0.017
P(7)	2696.801	2696.809	0.008	0.073	−0.017
P(6)	2697.535	2697.537	0.002	0.073	−0.016
P(5)	2698.270	2698.273	0.003	0.073	−0.016
P(4)	2699.005	2699.003	−0.002	0.073	−0.016
P(3)	2699.740	2699.748	0.008	0.074	−0.016
P(2)	2700.476	2700.464	−0.012	0.074	−0.016
P(1)	2701.212	2701.220	0.008	0.074	−0.016
R(0)	2702.685	2702.686	0.001	0.074	−0.016
R(3)	2704.897	2704.892	−0.005	0.071	−0.016
R(4)	2705.635	2705.618	−0.017	0.071	−0.016
R(5)	2706.374	2706.352	−0.022	0.071	−0.017
R(6)	2707.112	2707.094	−0.018	0.071	−0.017
R(7)	2707.851	2707.866	0.015	0.071	−0.017
R(8)	2708.591	2708.597	0.006	0.071	−0.018
R(9)	2709.330	2709.324	−0.006	0.072	−0.018
R(10)	2710.070	2710.065	−0.005	0.072	−0.018
R(11)	2710.811	2710.794	−0.017	0.072	−0.019
R(12)	2711.551	2711.534	−0.017	0.072	−0.019
R(13)	2712.292	2712.268	−0.024	0.072	−0.019
R(14)	2713.033	2713.019	−0.014	0.072	−0.019
R(15)	2713.774	2713.763	−0.011	0.073	−0.019
R(16)	2714.516	2714.498	−0.018	0.073	−0.019
R(17)	2715.257	2715.235	−0.022	0.073	−0.018
R(18)	2715.999	2715.982	−0.017	0.073	−0.018
R(19)	2716.742	2716.734	−0.008	0.073	−0.017
R(20)	2717.484	2717.481	−0.003	0.073	−0.016
R(21)	2718.226	2718.217	−0.009	0.073	−0.015
R(22)	2718.969	2718.953	−0.016	0.074	−0.014
R(23)	2719.712	2719.694	−0.018	0.074	−0.012
R(24)	2720.455	2720.446	−0.009	0.074	−0.010
R(25)	2721.198	2721.206	0.008	0.074	−0.008
R(26)	2721.941	2721.934	−0.007	0.074	−0.005
R(27)	2722.684	2722.686	0.002	0.074	−0.001
R(28)	2723.427	2723.413	−0.014	0.074	0.002
R(29)	2724.170	2724.168	−0.002	0.075	0.007
R(30)	2724.913	2724.933	0.020	0.075	0.011
R(31)	2725.657	2725.655	−0.002	0.075	0.017

[a] Calculated using spectroscopic parameters from Table 4.

Table 2
Measured and calculated line positions for the 21101–01101 band of CO_2 (628) obtained from SOIR spectra, and comparison with predictions available in HITRAN 2008 [16], which originate from [11].

Line	Calc.[a] (cm^{-1})	Obs. (cm^{-1})	Obs − Calc. (cm^{-1})	Obs. error (cm^{-1})	HITRAN − Calc. (cm^{-1})
$R_e(3)$	2794.483	2794.462	−0.021	0.073	−0.011
$R_e(4)$	2795.222	2795.220	−0.002	0.073	−0.011
$R_e(5)$	2795.960	2795.969	0.009	0.073	−0.012
$R_e(6)$	2796.699	2796.692	−0.007	0.073	−0.010
$R_e(7)$	2797.439	2797.448	0.009	0.074	−0.009
$R_e(8)$	2798.178	2798.177	−0.001	0.074	−0.008
$R_e(9)$	2798.918	2798.927	0.009	0.074	−0.008
$R_e(10)$	2799.658	2799.681	0.023	0.074	−0.007
$R_e(11)$	2800.398	2800.414	0.016	0.074	−0.006
$R_e(12)$	2801.139	2801.136	−0.003	0.074	−0.006
$R_e(13)$	2801.880	2801.849	−0.031	0.075	−0.005
$R_e(14)$	2802.621	2802.602	−0.019	0.075	−0.004
$R_e(15)$	2803.362	2803.365	0.003	0.075	−0.003
$R_e(16)$	2804.104	2804.107	0.003	0.075	−0.002
$R_e(17)$	2804.846	2804.852	0.006	0.075	−0.002
$R_e(18)$	2805.589	2805.589	−0.000	0.075	−0.001
$R_e(19)$	2806.332	2806.333	0.001	0.075	−0.000
$R_e(20)$	2807.075	2807.080	0.005	0.076	0.001
$R_e(21)$	2807.819	2807.825	0.006	0.076	0.001
$R_e(22)$	2808.563	2808.582	0.019	0.076	0.002
$R_e(23)$	2809.308	2809.307	−0.001	0.076	0.002
$R_e(24)$	2810.053	2810.045	−0.008	0.076	0.003
$R_e(25)$	2810.799	2810.797	−0.002	0.076	0.003
$R_e(26)$	2811.545	2811.533	−0.012	0.077	0.003
$R_e(27)$	2812.292	2812.278	−0.014	0.077	0.003
$R_e(28)$	2813.039	2813.032	−0.007	0.077	0.003
$R_e(29)$	2813.787	2813.799	0.012	0.077	0.002
$R_e(30)$	2814.535	2814.541	0.006	0.077	0.002
$R_e(31)$	2815.284	2815.285	0.001	0.077	0.001
$R_f(3)$	2794.487	2794.488	0.001	0.073	0.005
$R_f(4)$	2795.234	2795.249	0.015	0.073	0.005
$R_f(5)$	2795.983	2795.988	0.005	0.073	0.005
$R_f(6)$	2796.734	2796.751	0.017	0.073	0.005
$R_f(7)$	2797.486	2797.480	−0.006	0.074	0.005
$R_f(8)$	2798.241	2798.238	−0.003	0.074	0.005
$R_f(9)$	2798.997	2798.999	0.002	0.074	0.005
$R_f(10)$	2799.755	2799.749	−0.006	0.074	0.005
$R_f(11)$	2800.515	2800.522	0.007	0.074	0.005
$R_f(12)$	2801.277	2801.302	0.025	0.074	0.005
$R_f(13)$	2802.040	2802.040	0.000	0.075	0.005
$R_f(14)$	2802.806	2802.820	0.014	0.075	0.005
$R_f(15)$	2803.573	2803.579	0.006	0.075	0.005
$R_f(16)$	2804.342	2804.336	−0.006	0.075	0.004
$R_f(17)$	2805.113	2805.116	0.003	0.075	0.004
$R_f(18)$	2805.886	2805.890	0.004	0.075	0.004
$R_f(19)$	2806.661	2806.662	0.001	0.076	0.003
$R_f(20)$	2807.438	2807.419	−0.019	0.076	0.003
$R_f(21)$	2808.216	2808.202	−0.014	0.076	0.002
$R_f(22)$	2808.997	2808.984	−0.013	0.076	0.002
$R_f(23)$	2809.780	2809.778	−0.002	0.076	0.001
$R_f(24)$	2810.564	2810.561	−0.003	0.076	0.000
$R_f(25)$	2811.351	2811.360	0.009	0.076	−0.001
$R_f(26)$	2812.140	2812.144	0.004	0.077	−0.002
$R_f(27)$	2812.931	2812.930	−0.001	0.077	−0.003
$R_f(28)$	2813.724	2813.725	0.001	0.077	−0.005
$R_f(29)$	2814.519	2814.525	0.006	0.077	−0.006
$R_f(30)$	2815.316	2815.315	−0.001	0.077	−0.008

[a] Calculated using spectroscopic parameters from Table 4.

out of 137 for order 121. The calibration was performed using HDO lines, the positions of which being characterized by an accuracy $\geq 10^{-3}\,cm^{-1}$ and $< 10^{-2}\,cm^{-1}$ in HITRAN [16]. The wavenumber shift remaining between HITRAN and SOIR HDO lines used for calibration is around $8 \times 10^{-5}\,cm^{-1}$. As the precision of the measured line positions listed in Table 1 is around $7 \times 10^{-2}\,cm^{-1}$, their absolute uncertainty can therefore be estimated to be of the same magnitude. As was mentioned in the introduction, the R branch of the 20001–00001 band was observed by Villanueva et al. [10] in Mars spectra but incorrectly

Table 3
Measured and calculated line positions for the 01111–00001 band of CO_2 (628) obtained from SOIR spectra, and comparison with predictions available in HITRAN 2008 [16], which originate from [11] and with observations available in [8].

Line	Calc.[a] (cm^{-1})	Obs (cm^{-1})	Obs − Calc (cm^{-1})	Obs. error (cm^{-1})	HITRAN − Calc. (cm^{-1})	Obs[VW] − Obs[TW]
Q(68)–Q(70)						[b]
P(39)–P(59)						[b]
P(38)	2950.719	2950.780	0.061	0.077	−0.016	−0.040
P(37)	2951.636	2951.619	−0.017	0.077	−0.017	0.001
P(36)	2952.548	2952.550	0.002	0.077	−0.017	−0.050
P(35)	2953.455	2953.445	−0.010	0.078	−0.018	−0.025
P(34)	2954.358	2954.357	−0.001	0.078	−0.019	0.013
P(33)	2955.255	2955.281	0.026	0.078	−0.019	−0.061
P(32)	2956.148	2956.137	−0.011	0.078	−0.020	−0.037
P(31)	2957.036	2957.012	−0.024	0.078	−0.021	−0.032
P(30)	2957.919	2957.930	0.011	0.079	−0.022	−0.060
P(29)	2958.798	2958.766	−0.032	0.079	−0.022	0.014
P(28)	2959.671	2959.636	−0.035	0.079	−0.023	0.014
P(27)	2960.540	2960.543	0.003	0.079	−0.024	−0.060
P(26)	2961.403	2961.376	−0.027	0.079	−0.025	−0.056
P(25)	2962.262	2962.237	−0.025	0.080	−0.025	−0.037
P(24)	2963.116	2963.101	−0.015	0.080	−0.026	−0.040
P(23)	2963.966	2963.959	−0.007	0.080	−0.027	−0.029
P(22)	2964.810	2964.771	−0.039	0.080	−0.027	−0.041
P(21)	2965.649	2965.661	0.012	0.080	−0.028	−0.061
P(20)	2966.484	2966.470	−0.014	0.081	−0.029	−0.050
P(19)	2967.314	2967.317	0.003	0.081	−0.029	−0.017
P(18)	2968.139	2968.113	−0.026	0.081	−0.030	−0.023
P(17)	2968.959	2968.960	0.001	0.081	−0.030	−0.059
P(16)	2969.774	2969.762	−0.012	0.081	−0.031	−0.061
P(15)	2970.584	2970.599	0.015	0.081	−0.032	−0.069
P(14)	2971.389	2971.425	0.036	0.082	−0.032	−0.085
P(13)	2972.189	2972.182	−0.007	0.082	−0.033	−0.022
P(12)	2972.985	2973.018	0.033	0.080	−0.033	−0.108
P(11)	2973.776	2973.742	−0.034	0.078	−0.033	−0.022
Q(65)	2973.895	2973.918	0.023	0.078	−0.043	−0.088
Q(64)	2974.143	2974.159	0.016	0.078	−0.040	0.001
Q(63)	2974.388	2974.373	−0.015	0.078	−0.037	−0.013
P(10)	2974.561	2974.552	−0.009	0.078	−0.034	−0.022
Q(62)	2974.629	2974.620	−0.009	0.078	−0.035	−0.059
Q(61)	2974.866	2974.849	−0.017	0.078	−0.032	−0.039
Q(60)	2975.099	2975.093	−0.006	0.078	−0.030	0.017
Q(59)	2975.329	2975.344	0.013	0.078	−0.028	−0.074
P(9)	2975.342	2975.347	0.005	0.078	−0.034	0.003
Q(58)	2975.555	2975.532	−0.023	0.078	−0.026	0.000
Q(57)	2975.777	2975.800	0.023	0.078	−0.024	−0.050
Q(56)	2975.996	2975.997	0.001	0.078	−0.023	0.000
P(8)	2976.118	2976.112	−0.006	0.078	−0.034	−0.042
Q(55)	2976.210	2976.216	0.006	0.078	−0.021	−0.066
Q(54)	2976.421	2976.400	−0.021	0.078	−0.020	0.030
Q(53)	2976.628	2976.637	0.009	0.078	−0.019	−0.007
Q(52)	2976.832	2976.811	−0.021	0.078	−0.018	0.049
P(7)	2976.889	2976.894	0.005	0.078	−0.035	−0.024
Q(51)	2977.031	2977.024	−0.007	0.078	−0.017	−0.024
Q(50)	2977.227	2977.240	0.013	0.079	−0.016	−0.020
Q(49)	2977.419	2977.382	−0.037	0.079	−0.016	−0.032
Q(48)	2977.608	2977.597	−0.011	0.079	−0.015	−0.067
P(6)	2977.655	2977.653	−0.002	0.079	−0.035	0.007
Q(47)	2977.792	2977.811	0.019	0.079	−0.015	−0.061
Q(46)	2977.973	2977.975	0.002	0.079	−0.014	0.045
Q(45)	2978.150	2978.153	0.003	0.079	−0.014	−0.013
Q(44)	2978.323	2978.314	−0.009	0.079	−0.014	***
P(5)	2978.416	2978.428	0.012	0.079	−0.035	−0.048
Q(43)	2978.492	2978.493	0.001	0.079	−0.014	−0.033
Q(42)	2978.658	2978.641	−0.017	0.079	−0.014	−0.041
Q(41)	2978.820	2978.852	0.032	0.079	−0.014	−0.082
Q(40)	2978.977	2978.977	0.000	0.079	−0.014	−0.017
Q(39)	2979.132	2979.159	0.027	0.079	−0.015	0.001
P(4)	2979.172	2979.192	0.020	0.079	−0.035	−0.022
Q(38)	2979.282	2979.283	0.001	0.079	−0.015	−0.033
Q(37)	2979.428	2979.402	−0.026	0.079	−0.015	0.008
Q(36)	2979.571	2979.608	0.037	0.079	−0.016	−0.048
Q(35)	2979.710	2979.728	0.018	0.079	−0.016	−0.008

Table 3 (*continued*)

Line	Calc.[a] (cm^{-1})	Obs (cm^{-1})	Obs − Calc (cm^{-1})	Obs. error (cm^{-1})	HITRAN − Calc. (cm^{-1})	Obs[VW] − Obs[TW]
Q(34)	2979.845	2979.848	0.003	0.079	−0.017	0.002
P(3)	2979.923	2979.870	−0.053	0.079	−0.035	0.010
Q(33)	2979.976	2979.997	0.021	0.079	−0.017	0.023
Q(32)	2980.103	2980.098	−0.005	0.079	−0.018	0.022
Q(31)	2980.227	2980.234	0.007	0.079	−0.018	−0.004
Q(30)	2980.346	2980.338	−0.008	0.079	−0.019	***
Q(29)	2980.462	2980.444	−0.018	0.079	−0.020	−0.044
Q(28)	2980.574	2980.574	0.000	0.079	−0.020	***
P(2)	2980.669	2980.670	0.001	0.079	−0.035	0.000
Q(27)	2980.682	2980.690	0.008	0.079	−0.021	−0.020
Q(26)	2980.787	2980.782	−0.005	0.079	−0.021	−0.062
Q(25)	2980.887	2980.880	−0.007	0.079	−0.022	***
Q(24)	2980.984	2981.024	0.040	0.079	−0.023	***
Q(23)	2981.076	2981.077	0.001	0.079	−0.023	***
Q(22)	2981.165	2981.163	−0.002	0.079	−0.024	***
Q(21)	2981.250	2981.220	−0.030	0.079	−0.025	***
Q(20)	2981.332	2981.307	−0.025	0.079	−0.025	−0.007
Q(19)	2981.409	2981.383	−0.026	0.079	−0.026	***
Q(18)	2981.482	2981.490	0.008	0.079	−0.027	−0.030
Q(17)	2981.552	2981.558	0.006	0.079	−0.027	***
Q(16)	2981.618	2981.613	−0.005	0.079	−0.028	***
Q(15)	2981.680	2981.664	−0.016	0.079	−0.028	0.006
Q(14)	2981.738	2981.708	−0.030	0.079	−0.029	***
Q(13)	2981.792	2981.780	−0.012	0.079	−0.029	0.000
Q(12)	2981.842	2981.856	0.014	0.079	−0.030	−0.026
Q(11)	2981.889	2981.896	0.007	0.079	−0.030	***
Q(10)	2981.931	2981.935	0.004	0.079	−0.031	***
Q(9)	2981.970	2981.955	−0.015	0.079	−0.031	***
Q(8)	2982.005	2982.043	0.038	0.080	−0.031	***
Q(7)	2982.036	2982.063	0.027	0.080	−0.032	***
Q(6)	2982.063	2982.078	0.015	0.080	−0.032	***
Q(5)	2982.086	2982.091	0.005	0.080	−0.032	***
Q(4)	2982.105	2982.101	−0.004	0.080	−0.032	***
Q(3)	2982.121	2982.101	−0.020	0.080	−0.032	***
Q(2)	2982.133	2982.134	0.001	0.080	−0.033	***
Q(1)	2982.140	2982.134	−0.006	0.080	−0.033	***
R(0)	2982.878	2982.866	−0.012	0.080	−0.035	0.024
R(1)	2983.605	2983.620	0.015	0.080	−0.035	−0.070
R(2)	2984.326	2984.333	0.007	0.080	−0.035	−0.023
R(3)	2985.043	2985.045	0.002	0.080	−0.035	−0.024
R(4)	2985.755	2985.772	0.017	0.080	−0.035	−0.022
R(5)	2986.461	2986.459	−0.002	0.080	−0.035	−0.039
R(6)	2987.163	2987.176	0.013	0.080	−0.034	−0.026
R(7)	2987.860	2987.867	0.007	0.080	−0.034	−0.017
R(8)	2988.551	2988.573	0.022	0.079	−0.034	−0.063
R(9)	2989.238	2989.223	−0.015	0.079	−0.033	0.007
R(10)	2989.920	2989.949	0.029	0.079	−0.033	−0.059
R(11)	2990.597	2990.595	−0.002	0.079	−0.033	0.025
R(12)	2991.269	2991.291	0.022	0.079	−0.032	−0.011
R(13)	2991.936	2991.966	0.030	0.079	−0.032	−0.036
R(14)	2992.598	2992.616	0.018	0.079	−0.03	−0.016
R(15)	2993.254	2993.244	−0.010	0.079	−0.030	0.006
R(16)	2993.906	2993.945	0.039	0.079	−0.030	−0.025
R(17)	2994.553	2994.555	0.002	0.079	−0.029	0.045
R(18)	2995.195	2995.239	0.044	0.079	−0.029	−0.079
R(19)	2995.832	2995.826	−0.006	0.079	−0.028	−0.045
R(20)	2996.464	2996.444	−0.020	0.079	−0.027	−0.024
R(21)	2997.091	2997.063	−0.028	0.079	−0.027	0.007
R(22)	2997.713	2997.687	−0.026	0.079	−0.026	0.013
R(23)	2998.330	2998.332	0.002	0.079	−0.025	−0.012
R(24)	2998.942	2998.947	0.005	0.079	−0.025	−0.037
R(25)	2999.550	2999.515	−0.035	0.079	−0.024	0.015
R(26)	3000.152	3000.145	−0.007	0.079	−0.023	−0.045
R(27)	3000.749	3000.768	0.019	0.079	−0.022	−0.028
R(28)	3001.341	3001.308	−0.033	0.079	−0.022	−0.008
R(29)	3001.928	3001.945	0.017	0.079	−0.021	−0.015
R(30)	3002.510	3002.511	0.001	0.079	−0.020	−0.081
R(31)	3003.087	3003.069	−0.018	0.079	−0.019	−0.009
R(32)	3003.659	3003.664	0.005	0.079	−0.019	−0.044
R(33)	3004.226	3004.242	0.016	0.079	−0.018	−0.052

Table 3 (*continued*)

Line	Calc.[a] (cm^{-1})	Obs (cm^{-1})	Obs − Calc (cm^{-1})	Obs. error (cm^{-1})	HITRAN − Calc. (cm^{-1})	Obs[VW] − Obs[TW]
R(34)	3004.788	3004.772	−0.016	0.079	−0.017	−0.022
R(35)	3005.345	3005.311	−0.034	0.079	−0.017	0.039
R(36)	3005.897	3005.907	0.010	0.079	−0.016	−0.007
R(37)	3006.444	3006.453	0.009	0.079	−0.016	−0.073
R(38)	3006.986	3006.988	0.002	0.079	−0.015	0.012
R(39)	3007.523	3007.528	0.005	0.079	−0.014	−0.048
R(40)	3008.055	3008.051	−0.004	0.079	−0.014	0.019
R(41)	3008.582	3008.590	0.008	0.079	−0.014	0.020
R(42)	3009.104	3009.113	0.009	0.079	−0.013	−0.013
R(43)	3009.621	3009.629	0.008	0.079	−0.013	−0.039
R(44)	3010.133	3010.149	0.016	0.079	−0.012	−0.049
R(45)	3010.640	3010.669	0.029	0.079	−0.012	−0.079
R(46)	3011.142	3011.146	0.004	0.079	−0.012	***
R(47)	3011.639	3011.636	−0.003	0.079	−0.012	***
R(48)	3012.131	3012.163	0.032	0.079	−0.012	−0.053
R(49)	3012.618	3012.603	−0.015	0.079	−0.012	***
R(50)	3013.099	3013.101	0.002	0.078	−0.012	−0.031
R(51)	3013.576	3013.607	0.031	0.078	−0.012	***
R(52)	3014.048	3014.053	0.005	0.078	−0.013	***
R(53)	3014.515	3014.515	−0.000	0.078	−0.013	***
R(54)	3014.977	3014.984	0.007	0.078	−0.014	***
R(55)	3015.434	3015.409	−0.025	0.078	−0.014	***
R(56)	3015.886	3015.853	−0.033	0.078	−0.015	***
R(57)	3016.333	3016.299	−0.034	0.078	−0.016	***
R(58)	3016.775	3016.798	0.023	0.078	−0.017	***
R(59)	3017.212	3017.240	0.028	0.078	−0.018	***
R(60)	3017.644	3017.617	−0.027	0.078	−0.019	***

Obs[VW]–Obs[TW] are the differences between the line positions obtained by Wilquet et al [7] and in this work.

[a] Calculated using spectroscopic parameters from Table 4.

[b] Line not included in the fit.

*** Line not observed by Wilquet et al. [7].

assigned to the P branch (see Table 2 of [10]). We changed the P23–P3 assignment of [10] to R4–R24 in accordance with HITRAN [16], which originates from [11]. Fig. 4 depicts the differences between the observed line positions and those available in HITRAN [16] after reassignment. It can be seen that all positions reported herein are within the stated measurement uncertainty of $\pm 0.07\ cm^{-1}$. However, some systematic discrepancies are observed for the P branch. As they are absent in the R branch, of the order of our measurement uncertainty and more than an order of magnitude larger than the uncertainty of the HITRAN line positions [16], these discrepancies probably result from a calibration issue of the SOIR spectra.

b) *The 21101–01101 band of $^{16}O^{12}C^{18}O$*

This hot band is of Π–Π type. It should therefore exhibit R, P, and Q branches, each line being split into two components. Our simulations with SPECTRA predicted that the P branch, up to $J=30$, should be observed between 2770 and 2790 cm^{-1} (order 124), the Q branch should be found around 2791.5 cm^{-1} (edge of order 124), and the R branch should begin in order 124 and be mainly visible in order 125. Unfortunately, as shown in Fig. 5, the P and Q branches of interest could not be measured because they are overlapped by strong lines of HCl and HDO, and the very strong 20001–00001 band of $^{16}O^{12}C^{17}O$.

The R branch was observed in order 125 up to $J=31$, as shown in Fig. 6. 15 orbits out of 28 were used to determine the line positions, with a precision around $7\times10^{-2}\ cm^{-1}$. The calibration was made using the HCl (accuracy $\geq10^{-4}\ cm^{-1}$ and $<10^{-3}\ cm^{-1}$ in HITRAN [16]) and HDO lines (accuracy $\geq10^{-3}\ cm^{-1}$ and $<10^{-2}\ cm^{-1}$ in HITRAN [16]) observed in order 125. The wavenumber shift remaining between HITRAN and SOIR HCl and HDO lines used for calibration is around $12\times10^{-5}\ cm^{-1}$. The absolute uncertainty of the carbon dioxide line positions was therefore again estimated to be limited by the precision of measurement. The measured line positions, together with the corresponding uncertainties and assignments, are listed in Table 2.

The 21101–01101 band of $^{16}O^{12}C^{18}O$ is present in HITRAN [16]. Fig. 7 depicts the differences between the HITRAN calculated line positions and the positions measured in the present work. These differences are also listed in Table 2. It can be seen that all the differences are within the experimental precision and randomly scattered around zero.

c) *The 01111–00001 band of $^{16}O^{12}C^{18}O$*

This cold $\Pi-\Sigma^+$ band has already been reported by Wilquet et al. [8] and Villanueva et al. [9]. It extends over three orders, from order 131 up to order 133, i.e. from 2930 to 3013 cm^{-1}. We reanalyzed this band, neglecting order 131 which corresponds to high J lines of the P branch. These lines are indeed too weak to be observed reliably in the SOIR spectra. The line positions measured in this work, with a precision around $7\times10^{-2}\ cm^{-1}$, are presented in Table 3. They were calibrated using $H^{35}Cl$ and $H^{37}Cl$ lines. The wavenumber shift remaining

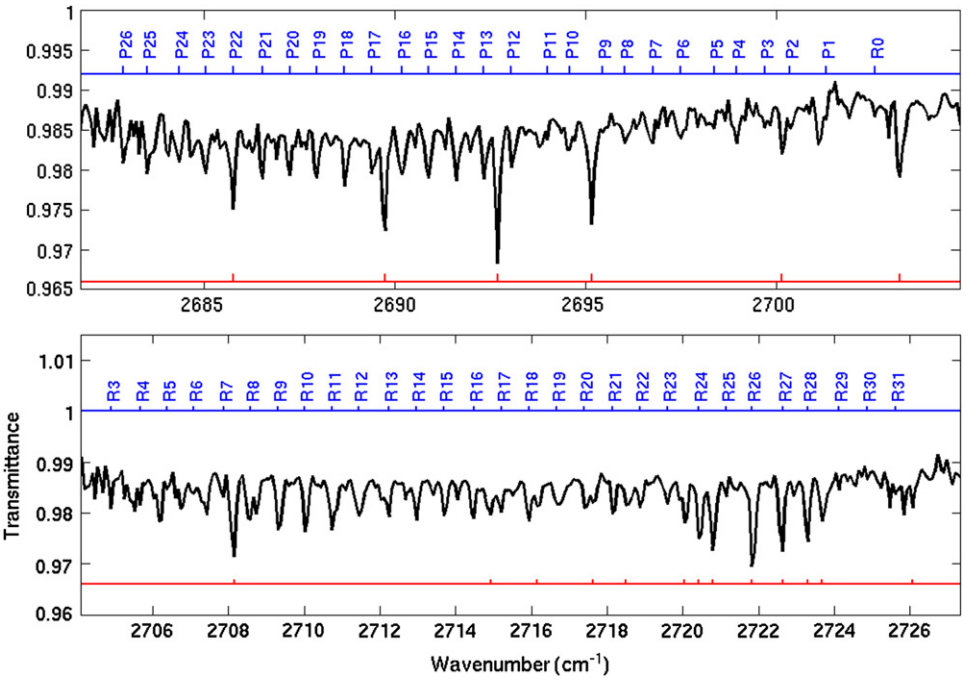

Fig. 3. Identification of the 20001–00001 band of CO_2 (638) in order 120 (upper panel) and 121 (lower panel). The positions and assignment of the carbon dioxide lines are indicated in the upper part of each panel. The lower markers identify HDO lines. The strongest of these lines were used for calibration purposes, using HITRAN [16] as reference.

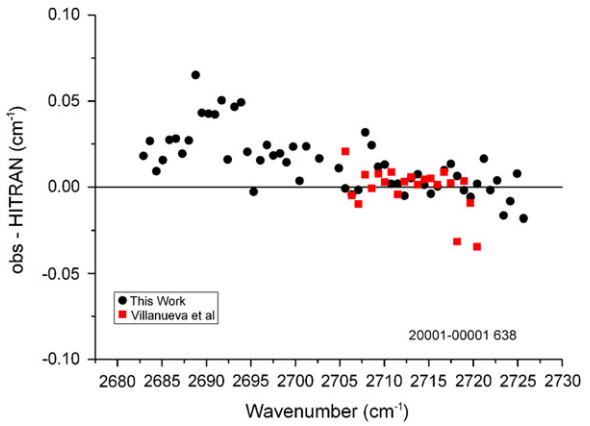

Fig. 4. Differences between line positions measured in this work and in [10] with HITRAN [16], for the 20001–00001 band of CO_2 (638).

between HITRAN and SOIR HCl lines used for calibration is around 4×10^{-5} cm^{-1}.

This band is also present in HITRAN [16]. Fig. 8 depicts the differences between the HITRAN calculated line positions and the observed positions from [8,9] and this work. Table 3 also includes the differences between HITRAN and [8] with this work. It can be seen that the differences involving [8,9] are randomly scattered around zero whereas the average of the differences involving this work is positive. Although the latter differences are smaller than the estimated measurement uncertainties, such a systematic discrepancy may again indicate some calibration problems in the present work.

3.3. Rotational analysis

Assuming that the vibrational states can be considered as isolated, the rovibrational energies in Σ^+ and Π states of a linear triatomic molecule can be expressed as

$$T(v,J)=G_v+B_v[J(J+1)-l_2^2]-D_vJ^2(J+1)^2+H_vJ^3(J+1)^3$$
$$=G_v-B_vl_2^2+F(J) \quad (1)$$

where G_v is the vibrational term value, and B_v, D_v and H_v are the rotational constants [12]. The positions of vibration–rotation lines can then be matched to the following expression:

$$\tilde{\nu}=T(v',J')-T(v'',J'')=\tilde{\nu}_c+F(J')-F(J'') \quad (2)$$

where $\tilde{\nu}_c=G_{v'}-B'_vl'_22-G_v+B''_vl''_22$ is the band origin, and primes and double primes refer to the upper and lower vibrational states, respectively. In the fitting procedures applied to the three bands analyzed in the present work, the band origin and the rotational constants B_v and D_v of the upper vibrational states were the only parameters fitted. The vibration–rotation constants of the ground and excited 01101 states of $^{16}O^{12}C^{18}O$ were respectively constrained to the values reported in [20] and [20,21], while those of the ground state of $^{16}O^{13}C^{18}O$ were fixed to the values given in [21]. As the sextic rotational constant H_v in the upper states was not determined within 3σ in the band by band fit, it was fixed to either zero (e and f sub-levels of the 21101 state of $^{16}O^{12}C^{18}O$ and 20001 of $^{16}O^{13}C^{18}O$) or to the value reported in [21] (e and f sub-levels of the 01111 state of $^{16}O^{12}C^{18}O$). In any case, if H_v is allowed to vary or fixed to zero, the corresponding changes the other parameters are within their estimated

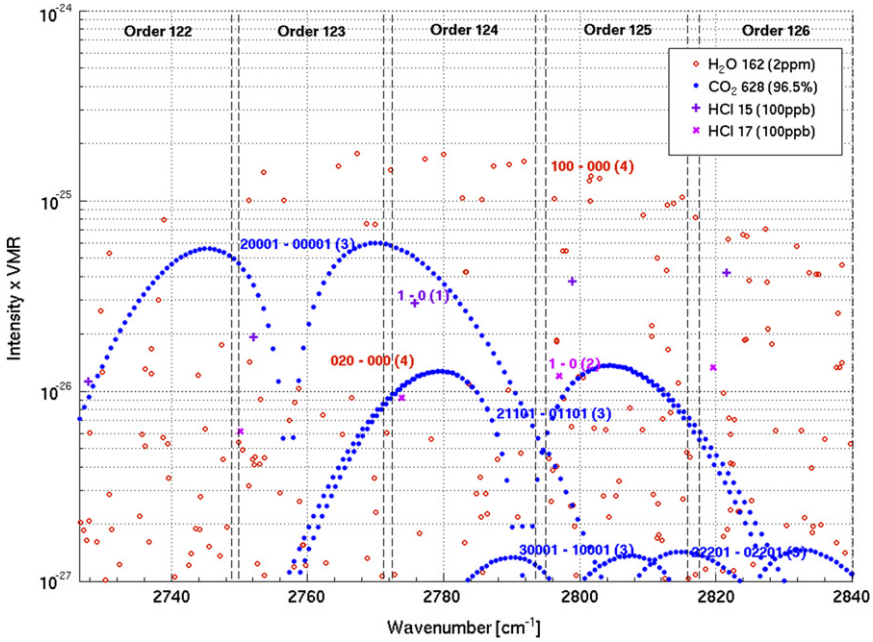

Fig. 5. Representation of the HDO, CO_2 (628), $H^{35}Cl$ and $H^{37}Cl$ spectra in orders 122–126, as available in the HITRAN 2008 database [16]. The P branch of CO_2 (628) hot band 21101–01101 is overlapped by the associated cold band and cannot be observed in the SOIR spectra. The volume mixing ratios (vmr) indicated in the legend correspond to the vmr of the molecule itself (all isotopologues mixed). Venusian isotopic ratio is taken into account to plot the graph, i.e. deuterium enriched water [19] and standard isotopic abundances for CO_2 and HCl. The numbers within parentheses, next to the vibrational identification, correspond to the isotopologue number.

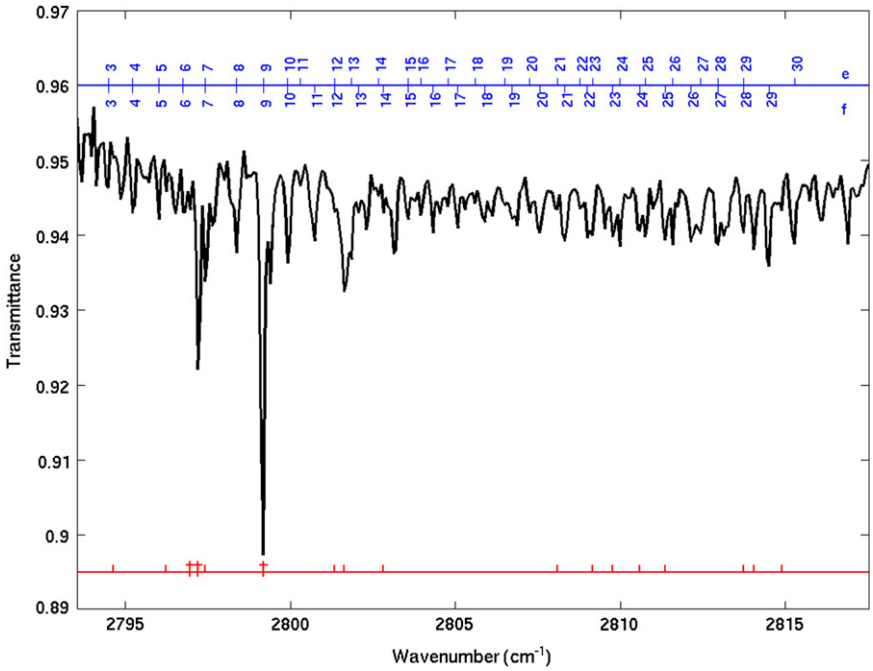

Fig. 6. Identification of the R-branch of the 21101–01101 band of CO_2 (628) in order 125. The positions and assignments of the carbon dioxide lines belonging to the band are indicated in the upper part of the figure. The lower markers identify HDO and HCl (†) lines. The strongest lines were used for calibration purposes, using HITRAN [16] as reference.

uncertainties. The ee and ff sub-bands of the 21101–01101 hot band of $^{16}O^{12}C^{18}O$ were considered independently.

The constants resulting from the fitting of observed line positions to Eqs. 1 and 2 are presented in Table 4, together with the literature values to which the fixed constants were constrained. The overall standard deviations of the fits are also given in Table 4, together with the number of line positions included. A few transitions

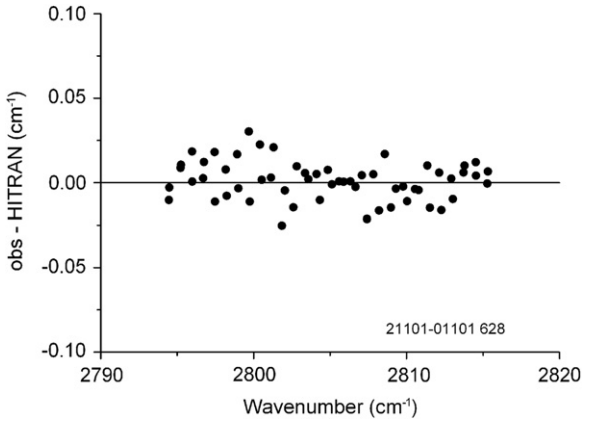

Fig. 7. Differences between line positions measured in this work and available in HITRAN [16] for the 21101–01101 band of CO_2 (628).

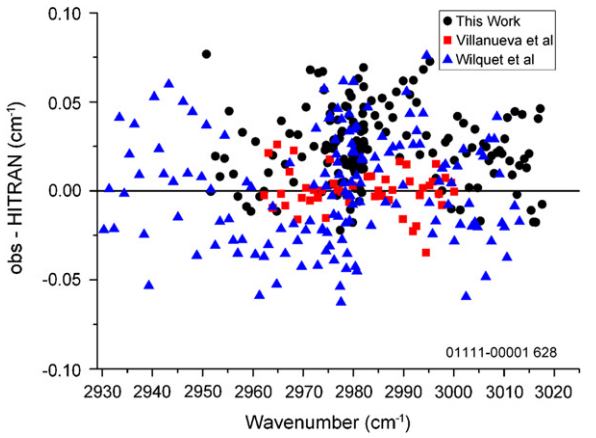

Fig. 8. Differences between line positions measured in this work, [8] and [9], and available in HITRAN [16] for the 01111–00001 band of CO_2 (628).

whose line positions differed from the corresponding calculated values by more than a chosen limit, i.e. 0.05 cm^{-1}, were excluded from the final cycle of the least-squares procedure.

Table 4 also includes the constants reported in the literature [10,21]. The vibration–rotation constants obtained in this work for the 01111e and 01111f states of $^{16}O^{12}C^{18}O$ are in good agreement with previous measurements [10,21], although the present value of D_v is about 3–5% lower than in [21]. Fig. 9 shows upper state rotational energies, calculated using the constants reported in this work and in [10,21], plotted versus $J(J+1)$. For better visibility, J values are used as ticks on the abscissa and the rovibrational energies, E_{VR}, are scaled using mean rotational B_m and quartic centrifugal distortion D_m constants according to:

$$E_{COR} = E_{VR} - B_m J(J+1) + D_m J^2(J+1)^2 \quad (3)$$

where B_m and D_m are calculated as the mean of rotational constants of the e and f sub-levels. Fig. 9 shows that the predicted rotational dependences are the same, but discrepancies up to about 0.2 cm^{-1} are observed at high J.

The present study involved the first observation of the 21101–01101 ($^{16}O^{12}C^{18}O$) band. Because its P and Q branches are heavily overlapped by the R-branch of the strong 20001–00001 band ($^{16}O^{12}C^{17}O$) (Section 3.2), the rotational analysis could only rely on the e- and f-components of the R-branch. Nevertheless Table 4 shows that the rotational and centrifugal distortion constants obtained in the present work are in good agreement with the predictions of Rothman et al. [21].

4. Conclusion

SOIR gathers information on the Venus atmosphere by looking at the sun through it as the satellite passes into and out of eclipse (i.e., solar occultation measurement). The instrument can measure from the top of the atmosphere (~170 km altitude) down to the top of the cloud layer

Table 4
Band centers, vibrational term values and rotational constants (in cm^{-1}) in CO_2.

Level	Type of band	v_c (cm^{-1})	G_v (cm^{-1})	B_v (cm^{-1})	$D_v \times 10^7$ (cm^{-1})	$H_v \times 10^{13}$ (cm^{-1})	Ref.[a]	B{$J_{min}J_{max}$}[b]	Number of lines	$\sigma \times 10^2$[c]
$^{16}O^{12}C^{18}O$										
00001				0.36818450	1.18647	−0.150	TO			
01101e			662.37335	0.36860192	1.20678	0.186	RT			
01101f			662.37335	0.36915324	1.20692	−0.285	RT			
01111e			2982.11105	0.36573112	1.20268	0.217	RT			
01111e	**Π–Σ$^+$ (GS)**	**2982.1230(35)**[d]		**0.3657130(65)**	**1.161(20)**	**0.217**[e]	**TW**	**P{2,38},R{0,60} R{0,60}**	**98**	**1.90**
01111f			2982.11105	0.36626757	1.20380	−0.296	RT			
01111f			2982.111	0.3663	1.20380[e]	−0.296[e]	GV			
01111f	**Π–Σ$^+$ (GS)**	**2982.1173(72)**		**0.3662470(95)**	**1.1396(23)**	**−0.296**[e]	**TW**	**Q{1,65}**	**65**	**2.20**
21101e			3454.011	0.368759	1.06	0.0	RT			
21101e	**Π–Π (v_2 e)**	**2791.5319(52)**		**0.3687270(27)**	**0.80(26)**	**0.0**[e]	**TW**	**R{3,31}**	**29**	**1.22**
21101f			3454.011	0.369167	1.12	0.0	RT			
21101f	**Π–Π (v_2 f)**	**2791.5155(55)**		**0.370048(31)**	**0.80(33)**	**0.0**[e]	**TW**	**R{1,30}**	**29**	**1.37**

Table 4 (*continued*)

Level	Type of band	v_c (cm^{-1})	G_v (cm^{-1})	B_v (cm^{-1})	$D_v \times 10^7$ (cm^{-1})	$H_v \times 10^{13}$ (cm^{-1})	Ref.[a]	B{$J_{min}J_{max}$}[b]	Number of lines	$\sigma \times 10^{2}$[c]
$^{16}O^{13}C^{18}O$										
00001				0.36818116	1.18498	0.000	RT			
20001			2722.62	0.3680(2404)	1.30	0.000[e]	GV	P{3,23}		
			2700.46	0.3683(2614)	–	–				
20001	**$\Sigma^+ - \Sigma^+$ (GS)**	**2701.9485(41)**		**0.368378(24)**	**1.71(26)**	**0.000[e]**	**TW**	**P{1,26},R{0,31} R{0,31}**	**56**	**1.62**

[a] References: TW—This Work; RT—Rothman et al. 1992 [21]; TO—Toth et al. 2007 [20]; GV—Villanueva et al. 2008 [10].
[b] $B\{J_{min}J_{max}\}$—branch identifier with the minimum and maximum observed angular momentum quantum numbers.
[c] σ is a standard deviation of a fit (cm^{-1}).
[d] The standard deviation (1σ) is given in parentheses in the unit of the last quoted digit.
[e] Constrained parameter.

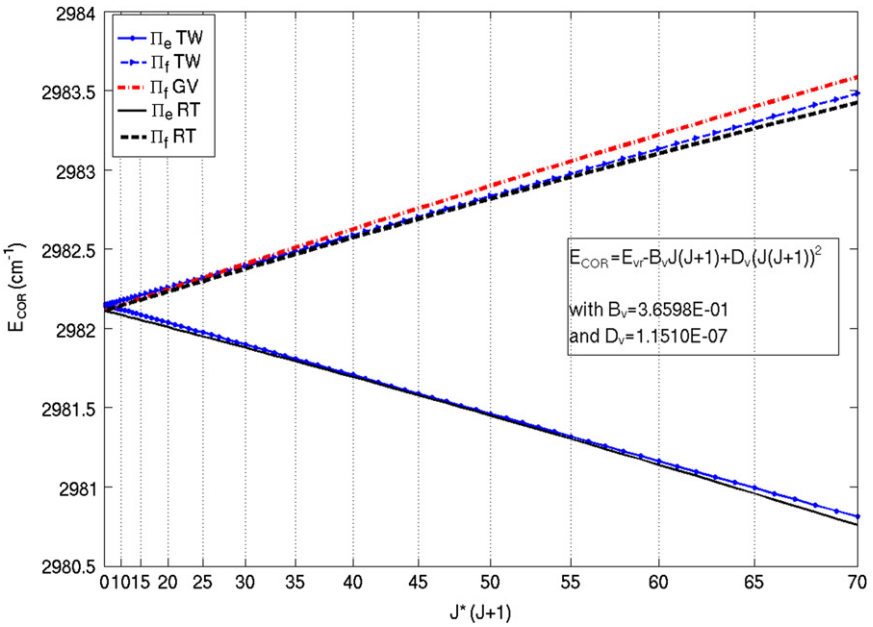

Fig. 9. Reduced vibration–rotation energies as a function of $J(J+1)$ for the 01111 state of CO_2 (628) located near 2982.12 cm^{-1}. For better visibility, J values are used as ticks on the abscissa The reduced energies (in cm^{-1}) are given by Eq. (3). Components of e and f symmetry are plotted as solid and dotted lines, respectively. TW: this work; GV: Villanueva et al. [10]; RT: Rothman et al. [21].

(~65 km). Given the high concentration of CO_2 in the Venus atmosphere, it is the ideal place to study the different isotopologues of the molecule, and their vibrational bands. The sensitivity of the SOIR instrument indeed allowed the detection of weak absorption bands of rare CO_2 isotopologues: the 20001–00001 band of $^{16}O^{13}C^{18}O$ and the 21101–01101 band of $^{16}O^{12}C^{18}O$ were observed and analyzed, and the analysis of the 01111–00001 band of $^{16}O^{12}C^{18}O$ was improved. The analysis of the 20001–00001 band of $^{16}O^{13}C^{18}O$ enabled us to dispel doubt about its identification in the Mars spectra [10]. The P23–P3 assignments of [10] should be changed to R4–R24 in agreement with the CDSD databank [11]. In addition, good agreement between observed SOIR spectra and spectra calculated using the predicted CO_2 lines available in the CDSD databank [11] demonstrated the precision of the latter information.

Additionally, weaker lines have yet to be identified in the range covered by the SOIR instrument. A systematic investigation is ongoing to assign all the lines and to further characterize them.

Acknowledgments

Venus Express is a planetary mission from the European Space Agency (ESA). We wish to thank all ESA members who participated in the mission, in particular H. Svedhem and O. Witasse. We thank our collaborators at IASB-BIRA/Belgium, LATMOS/France, and IKI/Russia. We thank CNES, CNRS, Roskosmos and the Russian Academy of Science. The research program was supported by the Belgian Federal Science Policy Office and the European Space Agency (ESA, PRODEX program, contracts C 90268,

90113, and 17645). Financial support from the *Fonds de la Recherche Scientifique* (F.R.S.–FNRS, contract FRFC) and the *Action de Recherches Concertées* of the *Communauté française de Belgique* is gratefully acknowledged. S. Robert thanks F. Tamassia, L. Fusina and G. Di Lonardo (Università di Bologna, Italy) for the band by band codes.

References

[1] Marov MY. Mikhail Lomonosov and the discovery of the atmosphere of Venus during the 1761 transit. In: Proceedings of the IAU colloquium. 2004;96:209–19.
[2] Adams WS, Dunham T. Absorption bands in the infrared spectrum of Venus. Publ Astron Soc Pac 1932;44:243–7.
[3] Bertaux JL, Nevejans D, Korablev O, Villard E, Quémerais E, Neefs E, et al. SPICAV on Venus Express: three spectrometers to study the global structure and composition of the Venus atmosphere. Planet Space Sci 2007;55:1673–700.
[4] Titov DV, Svedhem H, Koschny D, Hoofs R, Barabash S, Bertaux JL, et al. Venus Express science planning. Planet Space Sci 2006;54:1279–97.
[5] Nevejans D, Neefs E, Van Ransbeeck E, Berkenbosch S, Clairquin R, De Vos L, et al. Compact high-resolution space-borne echelle grating spectrometer with AOTF based on order sorting for the infrared domain from 2.2 to 4.3 μm. Appl Opt 2006;45:5191–206.
[6] Vandaele AC, De Mazière M, Drummond R, Mahieux A, Neefs E, Wilquet V, et al. Composition of the Venus mesosphere measured by SOIR on board Venus Express. J Geophys Res 2008;113:E00B23.
[7] Mandin J-Y. Interpretation of the CO_2 absorption bands observed in the Venus infrared spectrum between 1 and 2.5 μm. J Mol Spectrosc 1977;67:304–21.
[8] Wilquet V, Mahieux A, Vandaele AC, Perevalov VI, Tashkun SA, Fedorova A, et al. Line parameters for the 01111–00001 band of $^{12}C^{16}O^{18}O$ from SOIR measurements of the Venus atmosphere. J Quant Spectrosc Radiat Transfer 2008;109:895–905.
[9] Villanueva G, Mumma MJ, Novak R, Hewagama T. Identification of a new band system of isotopic CO_2 near 3.3 μm: Implications for remote sensing of biomarker gases on Mars. ICARUS 2008;195:34–44.
[10] Villanueva G, Mumma MJ, Novak R, Hewagama T. Discovery of multiple bands of isotopic CO_2 in the prime spectral regions used when searching for CH_4 and HDO on Mars. J Quant Spectrosc Radiat Transfer 2008;109:883–94.
[11] Perevalov VI, Tashkun SA. CDSD-296 (Carbon Dioxide Spectroscopic Databank): updated and enlarged version for atmospheric applications. In: Proceedings of the 10th HITRAN database conference. Cambridge, MA, USA; 2008. p. 13.
[12] Rothman LS, Young LDG. Infrared energy levels and intensities of carbon dioxide. J Quant Spectrosc Radiat Transfer 1981;25:505–24.
[13] Mahieux A, Berkenbosch S, Clairquin R, Fussen D, Mateshvili N, Neefs E, et al. In-flight performance and calibration of SPICAV/SOIR on-board Venus Express. Appl Opt 2008;47:2252–65.
[14] Mahieux A, Vandaele AC, Drummond R, Robert S, Wilquet V, Fedorova A, et al. Densities and temperatures in the Venus mesosphere and lower thermosphere retrieved from SOIR onboard Venus express: retrieval technique. J Geophys Res 2010;115:E12014.
[15] Mahieux A, Vandaele AC, Robert S, Wilquet V, Drummond R, Montmessin F, et al. Densities and temperatures in the Venus mesosphere and lower thermosphere retrieved from SOIR on board Venus express. Carbon dioxide measurements at the Venus terminator. J Geophys Res 2012;117:E07001.
[16] Rothman LS, Gordon IE, Barbe A, Benner DC, Bernath PF, Birk M, et al. The HITRAN 2008 molecular spectroscopic database. J Quant Spectrosc Radiat Transfer. 2009;110:533-572.
[17] Mikhailenko CN, Babikov YL, Golovko VF. Information-calculating system spectroscopy of atmospheric gases. The structure and main functions. Atmos Oceanic Opt 2005;18:685–95.
[18] Jacquinet-Husson N, Scott NA, Chédin A, Crépeau L, Armante R, Capelle V, et al. The GEISA spectroscopic database: current and future archive for Earth and planetary atmosphere studies. J Quant Spectrosc Radiat Transfer 2008;109:1043–59.
[19] Fedorova A, Korablev O, Vandaele AC, Bertaux JL, Belyaev D, Mahieux A, et al. HDO and H_2O vertical distributions and isotopic ratio in the Venus mesosphere by solar occultation at infrared spectrometer onboard Venus express. J Geophys Res 2008;113:E00B22.
[20] Toth RA, Miller CE, Brown LR, Devi VM, Benner C. Line positions and strengths of $^{16}O^{12}C^{18}O$, $^{18}O^{12}C^{18}O$ and $^{17}O^{12}C^{18}O$ between 2200 and 7000 cm^{-1}. J Mol Spectrosc 2007;243:43–61.
[21] Rothman LS, Hawkins RL, Wattson RB, Gamache RR. Energy levels, intensities, and linewidths of atmospheric carbon dioxide bands. J Quant Spectrosc Radiat Transfer 1992;48:537–66.